Three-Dimensional Photoacoustic Imaging Using a Two-Dimensional CMUT Array

Srikant Vaithilingam, *Student Member, IEEE*, Te-Jen Ma, *Student Member, IEEE*, Yukio Furukawa, *Member, IEEE*, Ira O. Wygant, *Student Member, IEEE*, Xuefeng Zhuang, *Student Member, IEEE*, Adam De La Zerda, Ömer Oralkan, *Member, IEEE*, Aya Kamaya, Sanjiv S. Gambhir, R. Brooke Jeffrey Jr., and Butrus T. Khuri-Yakub, *Fellow, IEEE*

***Abstract*—In this paper, we describe using a 2-D array of capacitive micromachined ultrasonic transducers (CMUTs) to perform 3-D photoacoustic and acoustic imaging. A tunable optical parametric oscillator laser system that generates nanosecond laser pulses was used to induce the photoacoustic signals. To demonstrate the feasibility of the system, 2 different phantoms were imaged. The first phantom consisted of alternating black and transparent fishing lines of 180 μm and 150 μm diameter, respectively. The second phantom comprised polyethylene tubes, embedded in chicken breast tissue, filled with liquids such as the dye indocyanine green, pig blood, and a mixture of the 2. The tubes were embedded at a depth of 0.8 cm inside the tissue and were at an overall distance of 1.8 cm from the CMUT array. Two-dimensional cross-sectional slices and 3-D volume rendered images of pulse-echo data as well as photoacoustic data are presented. The profile and beamwidths of the fishing line are analyzed and compared with a numerical simulation carried out using the Field II ultrasound simulation software. We investigated using a large aperture (64 × 64 element array) to perform photoacoustic and acoustic imaging by mechanically scanning a smaller CMUT array (16 × 16 elements). Two-dimensional transducer arrays overcome many of the limitations of a mechanically scanned system and enable volumetric imaging. Advantages of CMUT technology for photoacoustic imaging include the ease of integration with electronics, ability to fabricate large, fully populated 2-D arrays with arbitrary geometries, wide-bandwidth arrays and high-frequency arrays. A CMUT based photoacoustic system is proposed as a viable alternative to a piezoelectric transducer based photoacoustic systems.**

I. Introduction

Photoacoustic imaging (PAI), also called optoacoustic imaging, is a promising medical imaging technology because it combines the contrast information of optical imaging with the spatial resolution of acoustic imaging [1]. It is a non-ionizing and non-invasive imaging modality. Potential clinical applications for PAI include functional and molecular imaging as well as therapy monitoring [2]–[4]. In PAI, the target tissue is illuminated with short laser pulses that cause brief heating of absorbing structures such as blood vessels. The induced temperature increase generates acoustic pressure waves because of the thermoelastic effect. These pressure waves propagate to the surface of the tissue where they can be detected with ultrasound transducers. Those regions that are more optically absorbent than others will generate a stronger ultrasound signal. Using the ultrasound data, an image of the optical absorption properties of the tissue can be reconstructed.

Ultrasound transducer technology that has been optimized for PAI remains under development. The ideal acoustic transducer array should provide high axial and lateral resolution, strong sensitivity, wide bandwidth and not be affected by the exciting laser pulse [5]. If a whole 3-D photoacoustic image can be acquired in one laser pulse then a fast imaging frame rate can be achieved.

In this work, we propose using a 2-D capacitive micromachined ultrasonic transducer (CMUT) array to fulfill these requirements. Currently, experimental PAI systems typically use a single mechanically scanned focused piezoelectric transducer for detection of the laser-generated ultrasound. Using a CMUT array in place of a mechanically scanned element has several advantages. Because CMUTs are fabricated using a silicon micromachining process, 2-D arrays can be easily fabricated for a broad range of frequencies and sizes [6]. For a given aperture size, arrays make the data acquisition faster than using a single transducer. Arbitrary CMUT array geometries such as the ring array [7] as well as flexible arrays [8] have been demonstrated. A ring array allows for the laser light to come through the hole at the center of the array. In addition, CMUTs are easily integrated with electronics, either monolithically [9]–[11] or through flip-chip bonding [12]. Integrating electronics at the transducer level maximizes signal integrity and thus image quality. It also allows multiplexing of signals resulting in a reduced number of cables for interfacing with the signal processing system. CMUTs have wide bandwidth in immersion and a high efficiency [13], [14]. This is especially significant given the broadband nature of the laser-generated ultrasound.

Our goal is to develop a complete, real-time 3-D PAI system employing 2-D CMUT arrays that have been op-

Manuscript received March 3, 2009; accepted August 11, 2009. S. Vaithilingam was supported by a P. Michael Farmwald Stanford Graduate Fellowship. This research is supported by funds from Canon Inc. and also supported in part by grant NCI ICMIC P50 CA114747. Work was performed in part at the Stanford Nanofabrication Facility (a member of the National Nanotechnology Infrastructure Network), which is supported by the National Science Foundation under grant ECS-9731293, its lab members, and the industrial members of the Stanford Center for Integrated Systems.

S. Vaithilingam, T.-J. Ma, Y. Furukawa, I. O. Wygant, X. Zhuang, Ö. Oralkan, and B. T. Khuri-Yakub are with the Edward L. Ginzton Laboratory, Stanford University, Stanford, CA (e-mail: srikantv@stanford.edu).

A. De La Zerda and S. S. Gambhir are with the Department of Radiology, Molecular Imaging Program, Stanford University, Stanford, CA.

A. Kamaya and R. B. Jeffrey Jr. are with the Department of Radiology, Stanford University Medical Center, Stanford, CA.

Digital Object Identifier 10.1109/TUFFC.2009.1329

0885–3010/$25.00 © 2009 IEEE

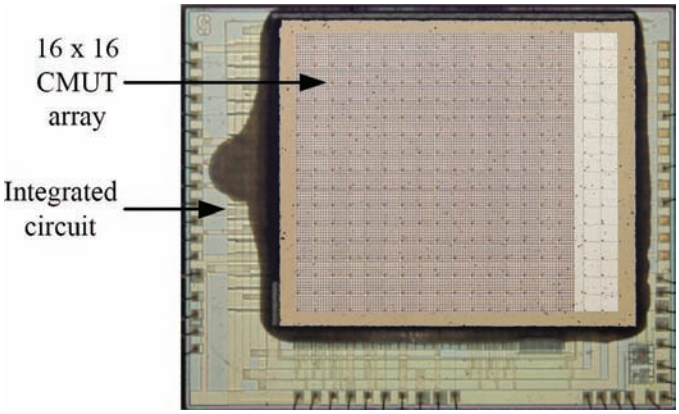

Fig. 1. Photograph of a 16 × 16 CMUT array flipchip bonded to a custom designed integrated circuit.

timized for PAI. Depending on the particular application, for example breast imaging or intravascular imaging, the configuration, size and shape of the array will be accordingly designed. While a complete system is our ultimate goal, in this paper we provide verification of our experimental setup and image reconstruction method, showing that CMUT arrays with integrated electronics are capable of 3-D PAI. We show images of a fishing-line phantom to demonstrate the resolution capabilities of the particular array used in these experiments and also corroborate these results with numerical simulation. Images from a second phantom comprising multiple tubes embedded in chicken breast tissue are also shown as such a phantom more closely mimics the conditions in living biological tissue. The tubes were filled with pig blood, indocyanine green (ICG) dye, and a mixture of both. ICG dye serves as a contrast agent to enhance photoacoustic detection [15]. This paper extends the results presented in earlier conference papers [16]–[19].

II. Methods

A. CMUT and Integrated Electronics

A 16 × 16 element CMUT array with integrated electronics was used to perform the experiments. Key parameters of this particular CMUT array are shown in Table I. The array was fabricated using a sacrificial layer etch process [6], [20]. The transducer array was flip-chip bonded to a custom-designed IC that comprises the front-end circuitry (Fig. 1). Integrating the electronics in this manner mitigates the effect of parasitic cable capacitance and simplifies connecting the transducer array to an external signal processing system by reducing the number of required cables. The IC provides a transmit and receive circuit to every element of the array. This circuit consists of a pulser, a low-noise transimpedance amplifier, a buffer to drive the output cable, and a switch that protects the low-voltage amplifier electronics from the pulser's output [12]. In this initial implementation, the IC allows only a single element to transmit and receive at a time. Thus, with no averaging, 256 pulses (one pulse per element) are required to acquire a single image.

TABLE I. CMUT Array Parameters.

Array size (elements)	16 × 16
Element pitch (μm)	250
CMUT membrane diameter (μm)	30
Number of membranes per element	36
Membrane thickness (μm)	0.5
Membrane material	Silicon nitride
Cavity thickness (μm)	0.1
Insulating layer thickness (μm)	0.15
Silicon substrate thickness (μm)	400
Flip-chip bond pad diameter (μm)	50
Through-wafer interconnect diameter (μm)	20
Silicon wafer resistivity (Ω-cm)	>10,000

We measured the output-referred noise of the complete flip-chip bonded device including preamplifier and buffer by connecting the buffer's output to a spectrum analyzer (Model 2712, Tektronix, Beaverton, OR) and recording the noise power as a function of frequency. An input-referred pressure noise or noise equivalent pressure (NEP) was determined by dividing the amplifier's output noise by the receive sensitivity of the CMUT element with integrated front-end electronics. For the receive sensitivity, an unfocused piezotransducer's (Panametrics A306S, Olympus NDT, Waltham, MA) output pressure was measured by a calibrated hydrophone (Onda HNP series, Onda Corporation, Sunnyvale, CA) at a fixed distance. Subsequently, the same piezotransducer was used as the pressure source for the CMUT array at the same distance. The measured output voltage of a CMUT element was divided by the pressure measured earlier from the hydrophone to determine the receive sensitivity. For the device used in these experiments, the NEP was calculated to be 2.6 mPa/$\sqrt{\text{Hz}}$ which is a little greater than the value reported in [12]. The CMUT array and IC were further characterized by immersing the array in oil and studying the pulse-echo signals from a plane-reflector. A typical A-scan taken from an oil-air interface, 1.3 cm away from the array, is shown in Fig 2(a). In this A-scan there are small perturbations following the main pulse. These signals might be caused by mechanical crosstalk between neighboring elements [21]. A polymer coating on the CMUT surface can be used to reduce mechanical cross-talk. The Fourier transform of the A-scan is shown in Fig 2(b). The center frequency is 3.48 MHz with a fractional bandwidth of 93.4%.

B. Experimental Setup

For these experiments, the phantom to be imaged was suspended in an acrylic tank of size 12 × 12 × 7 cm (Figs. 3 and 4). A rectangular hole was cut at the bottom of the tank. A ceramic package that contained the 16 × 16 element CMUT array (flip-chip bonded to an IC) was then glued to this hole. Vegetable oil was used to couple ultrasound between the CMUT array and phantom. Vegetable

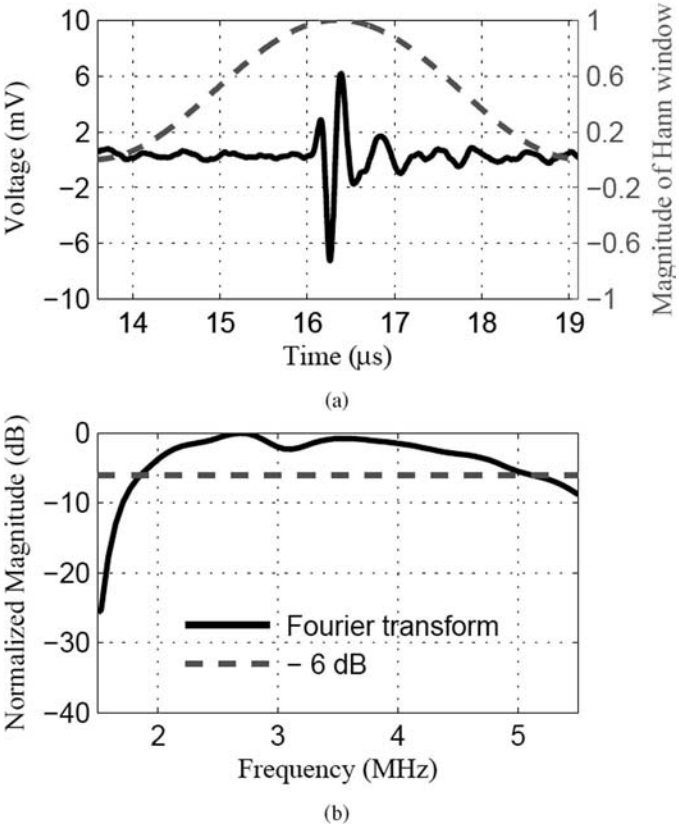

Fig. 2. Typical pulse-echo A-scan signal from a plane reflector at 1.3 cm and its Fourier transform. (a) The un-windowed pulse-echo A-scan taken from element at row 10, column 1. The Hann window applied to this A-scan before taking its Fourier transform is also shown. (b) Fourier transform of the windowed pulse-echo signal.

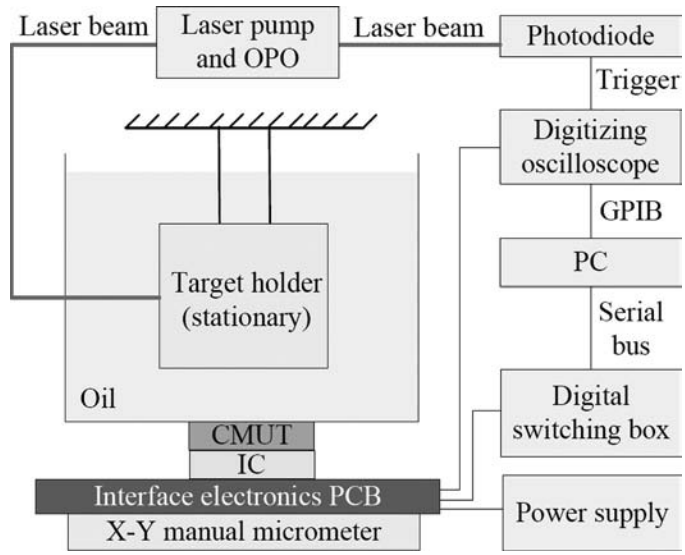

Fig. 3. Schematic of the experimental setup.

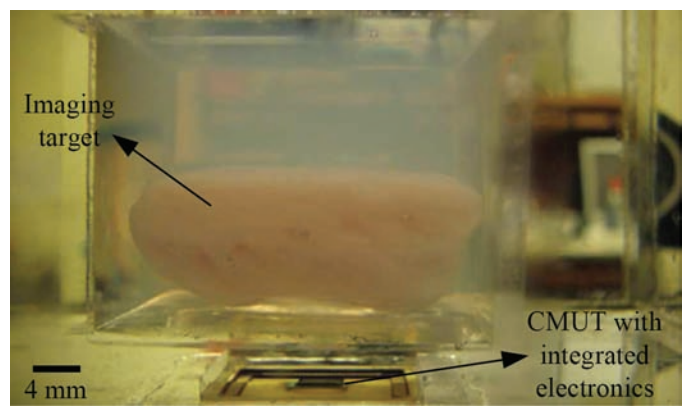

Fig. 4. Photograph of the experimental setup.

oil was used instead of water because it is nonconducting and thus allowed testing the device in immersion without the need to insulate the electronics. We have previously demonstrated CMUTs insulated with parylene and PDMS for operation in water as well as in direct contact with tissue [22], [23].

The CMUT array and tank were mounted on a precision x-y translational stage to enable planar scanning and emulation of a 64 × 64 element CMUT array. The method employed was as follows: After one data set was acquired, the array was translated 4 mm (length of the array) along the x-direction and another data set was acquired. Further data sets were obtained by translating 4 mm along the y-direction as well. In this manner, 16 total data sets were acquired. An image reconstructed from this data will be equivalent to that of an image reconstructed using a 64 × 64 element CMUT array. The phantom was illuminated from either one side or both sides of the tank (depending on the experiment) by a laser beam emitted from an optical parametric oscillator pumped by a Q-switched Nd:YAG laser (Model SLIII-10, Continuum, Santa Clara, CA). The laser pulses had a pulse-width of 5 ns and a repetition rate of 10 Hz. Free-space optics was used to guide the laser to the tank.

Two different phantoms were imaged. The first phantom was a resolution phantom consisting of 3 transparent 150 μm diameter fishing lines and 2 black 180 μm diameter fishing lines placed in an alternating pattern in planes parallel to the CMUT array. The basic geometry of the phantom is shown in Fig 5(a). We used single sided illumination for this phantom while gathering the photoacoustic data. The laser beam had a diameter of 2.5 cm, wavelength of 710 nm, and a fluence of 5.23 mJ/cm^2. The second phantom consisted of 4 polyethylene tubes embedded in chicken breast tissue. This phantom was designed to better mimic the conditions in living biological tissue. Chicken breast tissue was chosen because its optical absorption and scattering properties are similar to that of human breast tissue [24], [25]. The tissue was further embedded in a gel phantom made of agarose (Invitrogen, Carlsbad, CA). The gel phantom was used to easily suspend the phantom parallel to the CMUT array (Fig. 4). The inner diameter of the tubes was 1.19 mm and the outer diameter was 1.70 mm. The first tube was filled with deionized water; the second tube was filled with ICG solution in de-ionized water (5 μM); the third tube contained pig blood; the last tube was ICG mixed with pig blood

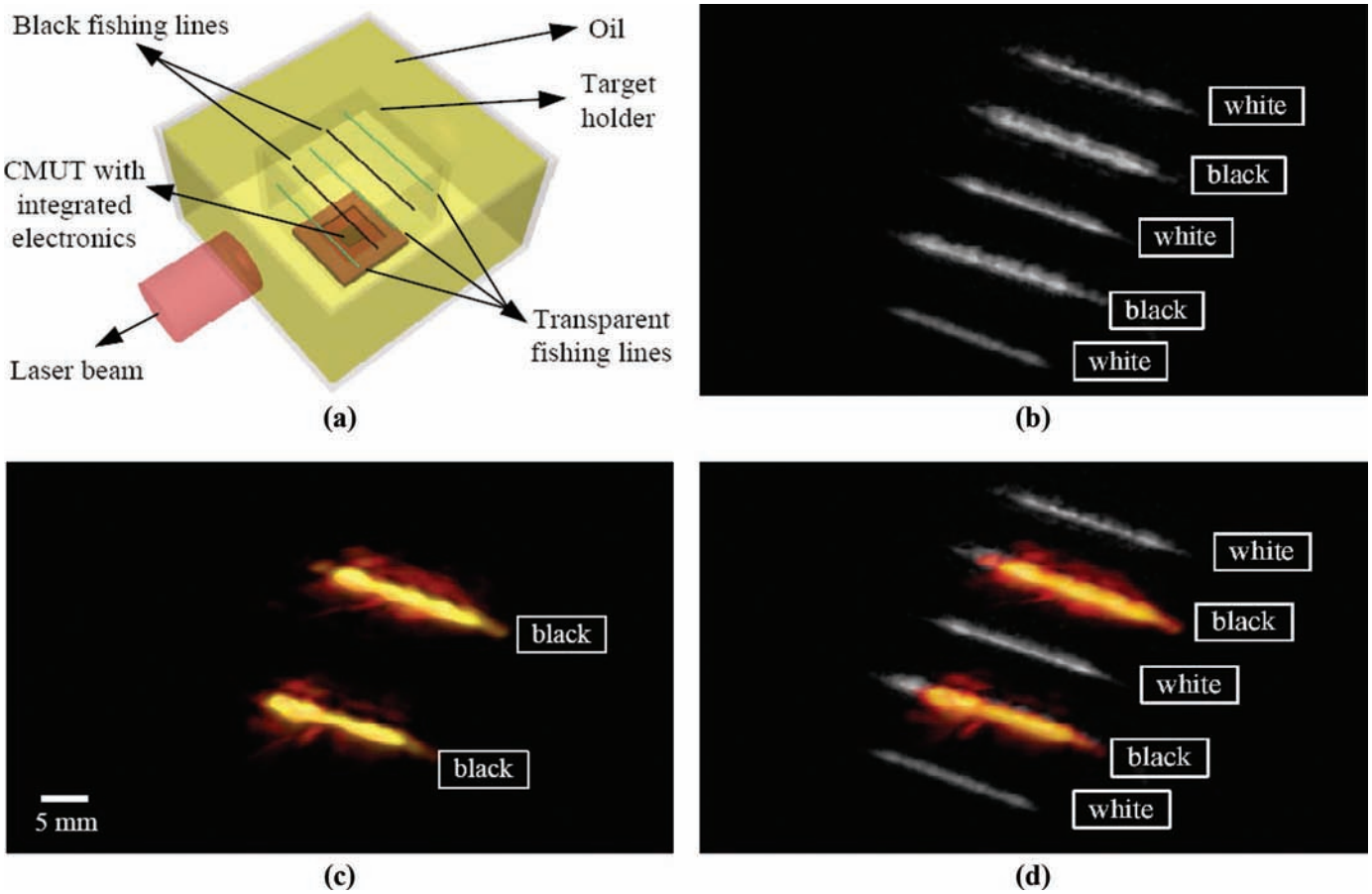

Fig. 5. Images of the fishing line phantom, reconstructed using the data from a 64 × 64 aperture. (a) Graphic of the fishing line phantom in the experimental setup. (b) 3-D rendered pulse-echo image displayed at 70 dB dynamic range. (c) 3-D rendered photoacoustic image displayed at 70 dB dynamic range. (d) 3-D rendered photoacoustic (hot-metal color scale) image overlaid on pulse-echo image (gray-scale) displayed at 70 dB dynamic range. References to color refer to the online version of this figure.

(5 μM). For the chicken phantom, we used double-sided laser illumination to achieve deeper light penetration in the tissue. Each laser beam had a diameter of 1.5 cm and a fluence of 8.99 mJ/cm^2 and 13.69 mJ/cm^2 respectively. We used a laser wavelength of 775 nm to gather the photoacoustic data because the peak ICG absorption is at this wavelength for the concentrations used [26].

C. Image Reconstruction

The images were reconstructed using the classical synthetic aperture (SA) focusing technique along with a coherence factor (CF) weighting [27]. Prior to image reconstruction, the A-scan from each element in the transducer array was filtered to eliminate out-of-band noise. These A-scans were then appropriately delayed and summed to form the image. The delays were calculated based upon the distance from the transducer element to the reconstructed point on the beam. Envelope detection was performed, in the end, after image reconstruction. This procedure can be expressed as

$$S_{\mathrm{SA}}(t) = \sum_{x,y=0}^{N_x-1,N_y-1} S_{xy}(t - \Delta t_{xy}), \tag{1}$$

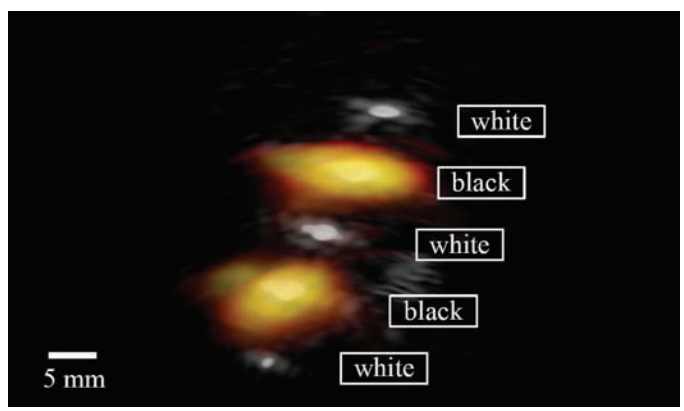

Fig. 6. 3-D rendered photoacoustic (hot-metal color scale) image overlaid on a pulse-echo image (gray-scale) displayed at 70 dB dynamic range; both reconstructed using the data from a 16 × 16 aperture. References to color refer to the online version of this figure.

where S_{SA} is the beamformed line before envelope detection, S_{xy} is the filtered a-scan that has been received at transducer element position (x, y), Δt_{xy} is the time delay applied to that signal, and N_x and N_y denote the total number of elements in the x and y directions. The beamformed image is then multiplied by a coherence factor weighting defined as follows:

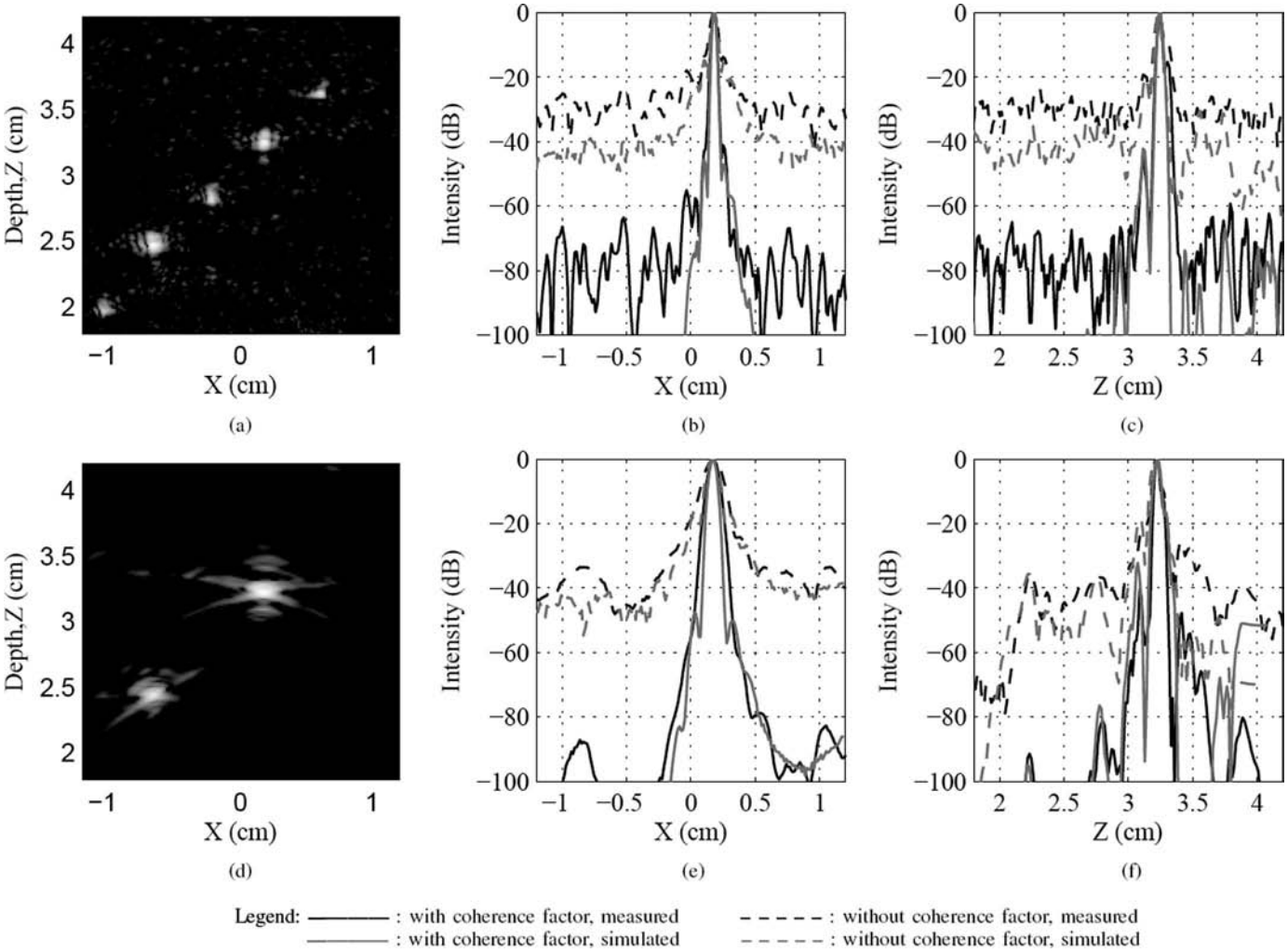

Fig. 7. (a) 2-D pulse-echo slice of fishing line phantom displayed at 70 dB dynamic range (from 64 × 64 aperture experimental data using coherence factor weighting). (b) Lateral pulse-echo line plot (normalized) of black fishing line at $z = 3.25$ cm. (c) Axial pulse-echo line plot (normalized) of black fishing line at $x = 0.19$ cm. (d) 2-D photoacoustic slice of fishing line phantom displayed at 70 dB dynamic range (from 64 × 64 aperture experimental data using coherence factor weighting). (e) Lateral photoacoustic line plot (normalized) of black fishing line at $z = 3.25$ cm. (f) Axial photoacoustic line plot (normalized) of black fishing line at $x = 0.19$ cm.

$$\mathrm{CF}(t) = \frac{\left| \sum_{x,y=0}^{N_x-1,N_y-1} S_{xy}(t - \Delta t_{xy}) \right|^2}{N_x N_y \cdot \sum_{x,y=0}^{N_x-1,N_y-1} \left| S_{xy}(t - \Delta t_{xy}) \right|^2}. \quad (2)$$

Note that the coherence factor weighting is multiplied on a point-by-point basis with the image obtained from synthetic aperture focusing. Using this weighting reduces focusing errors resulting from sound velocity inhomogeneities and other possible phase errors [28], [29]. The final photoacoustic and acoustic images are logarithmically compressed according to the dynamic range desired before being coregistered.

III. Results and Discussion

Conventional pulse-echo imaging data and PAI data were acquired for both phantoms. Medical image viewing software [30] was used to render the acquired volumetric images.

A. Fishing Line Phantom

The pulse-echo data was averaged 32 times to improve the SNR. The photoacoustic data was averaged 8 times. Volumetric images of the phantom, reconstructed using the 64 × 64 aperture data set, are shown in Fig. 5. In the pulse-echo image [Fig. 5(b)] all 5 fishing lines are seen because the color of the fishing lines is unimportant to the impinging pressure wave. However in the photoacoustic image [Fig.5(c)] only the 2 black fishing lines are apparent because the transparent fishing lines absorb very little light. The pulse-echo and photoacoustic images are co-registered and overlaid on each other as shown in Fig. 5(d). In the pulse-echo image, the 2 black fishing lines are thicker than the transparent fishing lines which is in good agreement with the fact that the black fishing lines have a 180 μm diameter as opposed to the transparent fishing

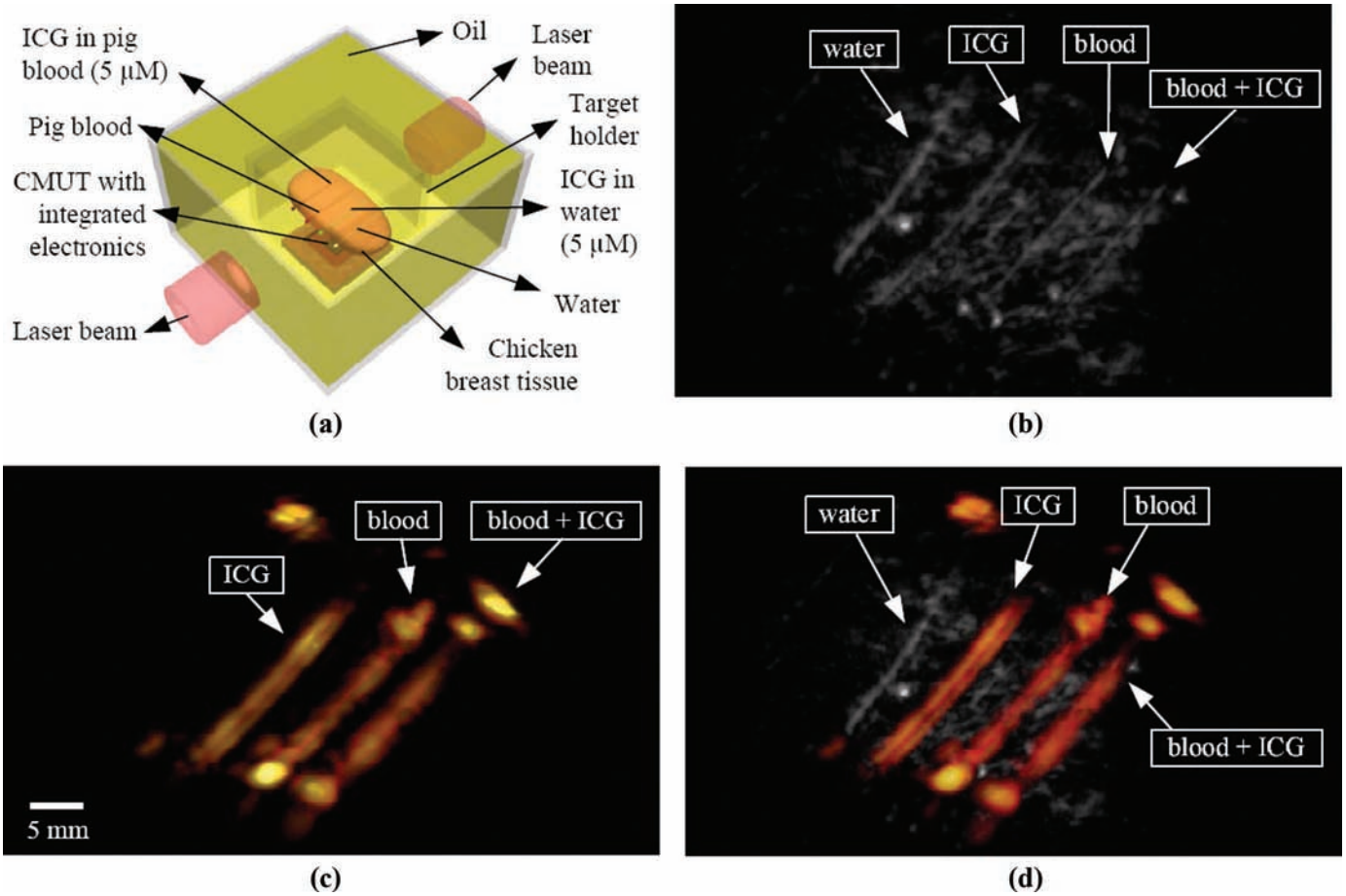

Fig. 8. Images of the chicken breast phantom, reconstructed using the data from a 64 × 64 aperture. (a) Graphic of tubes embedded in chicken breast phantom. (b) 3-D rendered pulse-echo image displayed at 70 dB dynamic range. (c) 3-D rendered photoacoustic image displayed at 70 dB dynamic range. (d) 3-D rendered photoacoustic (hot-metal color scale) image overlaid on pulse-echo image (gray-scale) displayed at 70 dB dynamic range. References to color refer to the online version of this figure.

lines, which have a 150 μm diameter. For comparison, the photoacoustic and pulse-echo images reconstructed using data from a 16 × 16 aperture is shown in Fig. 6. In Fig. 6, the wires are smeared and the lateral field of view is much reduced compared with the image reconstructed using the 64 × 64 aperture. 2-D pulse-echo and photoacoustic slices reconstructed from the 64 × 64 aperture data of the phantom are shown in Fig. 7(a) and Fig. 7(d), respectively.

The fishing line phantom image was also simulated using Field II, a program for simulating ultrasound fields [31], [32]. The resulting simulation data was then used to reconstruct an image using the same algorithm as described in Section II-C. For the photoacoustic simulation, an optical absorption distribution was assumed a priori to the ultrasound simulation. Using the reconstructed images, a comparison of the lateral and axial profiles of the upper black fishing line are shown in Fig. 7 (note, each line plot has been normalized for easy comparison) where we can see excellent agreement in the shape of the beam profiles. The measured lateral and axial beamwidths for both experimental and simulated images are shown in Table II. The lateral resolution in photoacoustic mode is worse than pulse-echo mode since we perform only receive beamforming in the former case. This is also why we compare the 3-dB beamwidths for photoacoustic images, but 6-dB beamwidths for pulse-echo images. In this experiment, another reason for the larger photoacoustic beamwidth could be reverberation of the black fishing line as seen in the images.

TABLE II. Measured Beamwidths From the Profile of the Black Fishing Line Located in the Upper Corner; Reconstructed Using 64 × 64 Aperture Data.

	Pulse-echo 6-dB beamwidth		Photoacoustic 3-dB beamwidth	
	Measured	Simulated	Measured	Simulated
Lateral (μm)	405	349	648	465
Axial (μm)	361	394	300	427

B. Chicken Breast Phantom

The pulse-echo data was averaged 64 times, whereas the photoacoustic data was averaged 8 times. Volumetric images of the phantom reconstructed using the 64 × 64 aperture data set are shown in Fig. 8. In the pulse-echo

image [Fig. 8(b)] all the 4 embedded tubes can be seen. However in the photoacoustic image [Fig. 8(c)] only 3 tubes are visible. The tubes filled with ICG, blood, and a mixture of the 2 can be seen, whereas the tube filled with de-ionized water is not visible. This is expected as at the wavelength of laser light used, 775 nm, water has a low absorption coefficient. The pulse-echo and photoacoustic images are co-registered and overlaid on each other as shown in Fig. 8(d). The tubes were embedded at a depth of 0.8 cm inside the tissue and were about 1.8 cm from the CMUT array surface. The SNR in the image between the 5 μM ICG tube and the background chicken breast tissue phantom was found to be 87 dB (after coherence factor weighting) in this particular experimental setup.

IV. Conclusion

We have demonstrated true 3-D PAI using 2-D CMUT arrays with integrated electronics. Images from a fishing line phantom and chicken breast phantom are shown. We showed how the image quality dramatically improves when a large aperture is used to perform the imaging. ICG at a concentration of 5 μM and pig blood were detected against a background of chicken tissue. All these experimental results are promising for the further development of CMUTs for PAI. We are currently working on fabricating a true 64 × 64 element array as well as improving our electronic ICs to receive signals from more than one element at a time to facilitate real-time imaging. In our future research we aim to image more complex phantoms as well as proceed to *in vivo* small animal imaging.

Acknowledgment

L. Randall provided valuable support for machining the experimental equipment. IC fabrication was provided by National Semiconductor (Santa Clara, CA).

References

[1] M. Xu and L. V. Wang, "Photoacoustic imaging in biomedicine," *Rev. Sci. Instrum.*, vol. 77, no. 4, art. no. 041101, 2006.

[2] A. De La Zerda, C. Zavaleta, S. Keren, S. Vaithilingam, S. Bodapati, Z. Liu, J. Levi, B. R. Smith, T.-J. Ma, Ö. Oralkan, Z. Cheng, X. Chen, H. Dai, B. T. Khuri-Yakub, and S. S. Gambhir, "Carbon nanotubes as photoacoustic molecular imaging agents in living mice," *Nat. Nanotechnol.*, vol. 3, no. 9, pp. 557–562, Sep. 2008.

[3] J. Shah, S. Park, S. Aglyamov, T. Larson, L. Ma, K. Sokolov, K. Johnston, T. Milner, and S. Y. Emelianov, "Photoacoustic imaging and temperature measurement for photothermal cancer therapy," *J. Biomed. Opt.*, vol. 13, no. 3, art. no. 034024 2008.

[4] M.-L. Li, J.-T. Oh, X. Xie, G. Ku, W. Wang, C. Li, G. Lungu, G. Stoica, and L. Wang, "Simultaneous molecular and hypoxia imaging of brain tumors in vivo using spectroscopic photoacoustic tomography," *Proc. IEEE*, vol. 96, no. 3, pp. 481–489, Mar. 2008.

[5] J. J. Niederhauser, M. Jaeger, and M. Frenz, "Real-time three-dimensional optoacoustic imaging using an acoustic lens system," *Appl. Phys. Lett.*, vol. 85, no. 5, pp. 846–848, 2004.

[6] A. S. Ergun, Y. Huang, X. Zhuang, Ö. Oralkan, G. G. Yaralioglu, and B. T. Khuri-Yakub, "Capacitive micromachined ultrasonic transducers: Fabrication technology," *IEEE Trans. Ultrason. Ferroelectr. Freq. Control*, vol. 52, no. 12, pp. 2242–2258, 2005.

[7] D. T. Yeh, Ö. Oralkan, I. O. Wygant, M. O'Donnell, and B. T. Khuri-Yakub, "3-D ultrasound imaging using a forward-looking CMUT ring array for intravascular/intracardiac applications," *IEEE Trans. Ultrason. Ferroelectr. Freq. Control*, vol. 53, no. 6, pp. 1202–1211, 2006.

[8] X. Zhuang, D. Lin, Ö. Oralkan, and B. T. Khuri-Yakub, "Fabrication of flexible transducer arrays with through-wafer electrical interconnects based on trench refilling with pdms," *J. Microelectromech. Syst.*, vol. 17, no. 2, pp. 446–452, 2008.

[9] C. Daft, S. Calmes, D. da Graca, K. Patel, P. Wagner, and I. Ladabaum, "Microfabricated ultrasonic transducers monolithically integrated with high voltage electronics," in *IEEE Ultrasonics Symp.*, vol. 1, Aug. 2004, pp. 493–496.

[10] P. C. Eccardt and K. Niederer, "Micromachined ultrasound transducers with improved coupling factors from a CMOS compatible process," *Ultrasonics*, vol. 38, pp. 774–780, 2000.

[11] R. Noble, R. Davies, D. King, M. Day, A. Jones, J. McIntosh, D. Hutchins, and P. Saul, "Low-temperature micromachined cMUTs with fully-integrated analogue front-end electronics," in *IEEE Ultrasonics Symp.*, vol. 2, Oct. 2002, pp. 1045–1050.

[12] I. Wygant, X. Zhuang, D. Yeh, Ö. Oralkan, A. Ergun, M. Karaman, and B. T. Khuri-Yakub, "Integration of 2D CMUT arrays with front-end electronics for volumetric ultrasound imaging," *IEEE Trans. Ultrason. Ferroelectr. Freq. Control*, vol. 55, no. 2, pp. 327–342, February. 2008.

[13] I. Ladabaum, X. C. Jin, H. T. Soh, A. Atalar, and B. T. Khuri-Yakub, "Surface micromachined capacitive ultrasonic transducers," *IEEE Trans. Ultrason. Ferroelectr. Freq. Control*, vol. 45, no. 3, pp. 678–690, 1998.

[14] G. G. Yaralioglu, A. S. Ergun, B. Bayram, E. Haeggstrom, and B. T. Khuri-Yakub, "Calculation and measurement of electromechanical coupling coefficient of capacitive micromachined ultrasonic transducers," *IEEE Trans. Ultrason. Ferroelectr. Freq. Control*, vol. 50, no. 4, pp. 449–456, 2003.

[15] G. Ku and L. V. Wang, "Deeply penetrating photoacoustic tomography in biological tissues enhanced with an optical contrast agent," *Opt. Lett.*, vol. 30, no. 5, pp. 507–509, 2005.

[16] I. O. Wygant, X. Zhuang, P. S. Kuo, D. T. Yeh, Ö. Oralkan, and B. T. Khuri-Yakub, "Photoacoustic imaging using a two-dimensional CMUT array," in *IEEE Ultrasonics Symp.*, Sep. 2006, pp. 1921–1924.

[17] S. Vaithilingam, I. O. Wygant, P. S. Kuo, X. Zhuang, Ö Oralkan, P. D. Olcott, and B. T. Khuri-Yakub, "Capacitive micromachined ultrasonic transducers (CMUTs) for photoacoustic imaging," *Proc. SPIE*, vol. 6086, no. 1, art. no. 608603, 2006.

[18] S. Vaithilingam, I. O. Wygant, S. Sifferman, X. Zhuang, Y. Furukawa, Ö Oralkan, S. Keren, S. S. Gambhir, and B. T. Khuri-Yakub, "Tomographic photoacoustic imaging using capacitive micromachined ultrasonic transducer (CMUT) technology," in *IEEE Ultrasonics Symp.*, Oct. 2006, pp. 397–400.

[19] S. Vaithilingam, T.-J. Ma, Y. Furukawa, Ö Oralkan, A. Kamaya, K. Torashima, M. Kupnik, I. O. Wygant, X. Zhuang, R. B. Jeffrey, Jr., and B. T. Khuri-Yakub, "Investigating large 2D arrays for photoacoustic and acoustic imaging using CMUT technology," in *IEEE Ultrasonics Symp.*, Nov. 2008, pp. 1238–1241.

[20] X. Jin, I. Ladabaum, and B. T. Khuri-Yakub, "The microfabrication of capacitive ultrasonic transducers," *J. Microelectromech. Syst.*, vol. 7, no. 3, pp. 295–302, Sep. 1998.

[21] D. H. Turnbull and F. S. Foster, "Fabrication and characterization of transducer elements in two-dimensional arrays for medical ultrasound imaging," *IEEE Trans. Ultrason. Ferroelectr. Freq. Control*, vol. 39, no. 4, pp. 464–475, Jul. 1992.

[22] X. Zhuang, A. Nikoozadeh, M. A. Beasley, G. G. Yaralioglu, B. T. Khuri-Yakub, and B. L. Pruitt, "Biocompatible coatings for CMUTs in a harsh, aqueous environment," *J. Micromech. Microeng.*, vol. 17, no. 5, pp. 994–1001, 2007.

[23] A. Nikoozadeh, I. Wygant, D.-S. Lin, O. Oralkan, A. Ergun, K. Thomenius, A. Dentinger, D. Wildes, G. Akopyan, K. Shivkumar, A. Mahajan, D. Stephens, D. Sahn, and P. Khuri-Yakub, "Fully integrated CMUT-based forward-looking intracardiac imaging for

electrophysiology," in *IEEE Ultrasonics Symp.*, Oct. 2007, pp. 900–903.

[24] P. Taroni, A. Pieri, A. Torricelli, D. Comelli, and R. Cubeddu, "In vivo absorption and scattering spectroscopy of biological tissues," *Photochem. Photobiol. Sci.*, vol. 2, pp. 124–129, 2003.

[25] G. Marquez, L. V. Wang, S.-P. Lin, J. A. Schwartz, and S. L. Thomsen, "Anisotropy in the absorption and scattering spectra of chicken breast tissue," *Appl. Opt.*, vol. 37, no. 4, pp. 798–804, 1998.

[26] C. Haritoglou, W. Freyer, S. G. Priglinger, and A. Kampik, "Light absorbing properties of indocyanine green (ICG) in solution and after adsorption to the retinal surface – an ex-vivo approach," *Graefes Arch. Clin. Exp. Ophthalmol.*, vol. 244, pp. 1196–1202, Sep. 2006.

[27] K. Hollman, K. Rigby, and M. O'Donnell, "Coherence factor of speckle from a multi-row probe," in *IEEE Ultrasonics Symp.*, vol. 2, 1999, pp. 1257–1260.

[28] P.-C. Li and M.-L. Li, "Adaptive imaging using the generalized coherence factor," *IEEE Trans. Ultrason. Ferroelectr. Freq. Control*, vol. 50, no. 2, pp. 128–141, Feb. 2003.

[29] C.-K. Liao, M.-L. Li, and P.-C. Li, "Optoacoustic imaging with synthetic aperture focusing and coherence weighting," *Opt. Lett.*, vol. 29, no. 21, pp. 2506–2508, 2004.

[30] O. Faha, "Osirix: An open source platform for advanced multimodality medical imaging," in *4th Int. Conf. Information and Communications Technology*, Dec. 2006, pp. 1–2.

[31] J. Jensen and N. Svendsen, "Calculation of pressure fields from arbitrarily shaped, apodized, and excited ultrasound transducers," *IEEE Trans. Ultrason. Ferroelectr. Freq. Control*, vol. 39, no. 2, pp. 262–267, Mar. 1992.

[32] J. A. Jensen, "Field: A program for simulating ultrasound systems," *Med. Biol. Eng. Comput.*, vol. 34, suppl. 1, pt. 1, pp. 351–353, 1996.

Srikant Vaithilingam received his B.S. degree in electrical engineering and his B.A. degree in mathematics from the University of Southern California, Los Angeles, CA, in 2003. He received his M.S. degree in electrical engineering from Stanford University, Stanford, CA, in 2006 and is currently pursuing a Ph.D. degree in electrical engineering at Stanford University. Srikant was a recipient of the USC Trustee scholarship and the Stanford Graduate Fellowship. His current research interests include ultrasonic and photoacoustic medical imaging, image reconstruction algorithms, and MEMS device fabrication.

Te-Jen Ma received his B.S. degree in mechanical engineering from National Taiwan University, Taipei, Taiwan, in 2004. He is currently working toward his Ph.D. degree in mechanical engineering at Stanford University, Stanford, CA. His research interests include photoacoustic medical imaging, micro-electro-mechanical systems (MEMS), and product design.

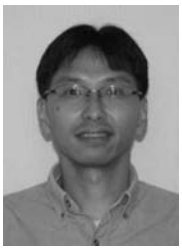

Yukio Furukawa received his B.S. and M.S. degrees from Osaka University, Osaka, Japan, in 1988 and 1990, respectively, both in electrical engineering. He entered Canon Inc., Japan, in 1990. He was a visiting scholar at Stanford University from 2006 to 2009. His past and present research interests include semiconductor laser device fabrication, design and modulation of second-harmonic generation lasers, and photoacoustic medical imaging.

Ira O. Wygant received his B.S. degree in electrical engineering with a cross-college major in computer science from the University of Wyoming, Laramie, WY, in 1999. He received his M.S. degree in electrical engineering from Stanford University, Stanford, CA, in 2002 and his Ph.D. degree in electrical engineering from Stanford University in 2008. After finishing his Ph.D., he joined National Semiconductor's research labs in Santa Clara, CA. His research interests include integrated circuit design, ultrasound imaging, and MEMs design and fabrication as they relate to capacitive micromachined ultrasound transducers.

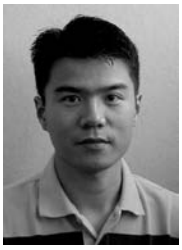

Xuefeng (Steve) Zhuang received the B.S. degree in 2002 from Louisiana State University, Baton Rouge, LA, and the M.S. and Ph.D. degrees from Stanford University, Stanford, CA, in 2004 and 2008, respectively, all in electrical engineering. He is currently with Kolo Technologies, Inc., where he is responsible for new technology development. His research interests include micromachined sensors and actuators for medical and industrial applications. He was a Stanford Graduate Fellow. He won the LSU University Medal and, in 2002, the McLaughlin Dean's Medal.

Adam de la Zerda is a Ph.D. candidate at the Stanford University Department of Electrical Engineering. He works on photoacoustic molecular imaging and its application for cancer imaging under the mentorship of Prof. Sanjiv Sam Gambhir. Mr. de la Zerda has received numerous awards for his work including the Best Poster Presentation at SPIE Photonics West 2009, Young Investigator Award at the World Molecular Imaging Congress 2008, the DoD Breast Cancer Research Award for predoctoral researchers, the Bio-X Graduate Student Fellowship, and first place at the Bay Area Entrepreneurship Contest. He holds a number of patents and publications in leading journals including *Nature*, *Nanotechnology*, and *Proceedings of the National Academy of Sciences*. Mr. de la Zerda studied Computer Engineering and Physics at the Technion–Israel Institute of Technology where he graduated with a B.Sc. degree Summa Cum Laude.

Ömer Oralkan received the B.S. degree from Bilkent University, Ankara, Turkey, in 1995, the M.S. degree from Clemson University, Clemson, SC, in 1997, and the Ph.D. degree from Stanford University, Stanford, CA, in 2004, all in electrical engineering. He joined the research staff at the E. L. Ginzton Laboratory of Stanford University in 2004 as an Engineering Research Associate. He was promoted to the rank of Senior Research Engineer in 2007. His past and present research interests include analog and digital circuit design, semiconductor device physics and fabrication, micromachined sensors and actuators, and medical imaging. His current research focuses on the design and implementation of integrated systems for catheter-based medical imaging applications, photoacoustic imaging, and chemical and biological sensor arrays. Dr. Oralkan has authored and co-authored over 100 publications and received the 2002 Outstanding Paper Award of the IEEE Ultrasonics, Ferroelectrics, and Frequency Control Society.

Aya Kamaya completed medical school at the University of Utah in her hometown of Salt Lake City, and obtained her Bachelor's degree in engineering sciences at Dartmouth College in Hanover, NH. She is an Assistant Professor of Radiology at Stanford University in the Abdominal Imaging Section. Since completion of her fellowship in body imaging at Stanford in 2005, she has been a Clinical Instructor and Clinical Assistant Professor in the Abdominal Imaging Section at Stanford. During this time, she was given two teaching awards for her dedication to resident education. She is currently the Associate Fellowship Director of the Stanford Body Imaging Fellowship. Prior to coming to Stanford for her fellowship, she completed her residency in Diagnostic Radiology at the University of Michigan in Ann Arbor, during which time she was awarded the Executive Council Award from the American Roentgen Ray Society for her work on "Twinkling Artifacts in Ultrasound Imaging," and the Laurence A. Mack Research Award from the Society of Radiologists in Ultrasound for her work on "Linear Streak Artifacts." Her research interests include photoacoustic imaging, liver imaging, and women's imaging.

Sanjiv S. Gambhir is a Professor of Radiology and Bioengineering at Stanford University. He is Director of the Molecular Imaging Program and Head of Nuclear Medicine. His laboratory has a long-standing interest in developing assays for multimodality molecular imaging of living subjects, including most recently the use of photoacoustic molecular imaging. Dr. Gambhir's laboratory has developed assays to interrogate molecular and cellular events in living subjects including gene expression and protein-protein interactions. He is the co-author of over 300 publications and 20 approved/pending patents. His recent awards include the Tesla Medal, the Hounsfield Medal, and election to the Institutes of Medicine of the National Academies.

R. Brooke Jeffrey, Jr., completed his Radiology residency at the University of California, San Francisco, and was a faculty member at UCSF from 1980 to 1989. In 1990, Dr. Jeffrey moved to Stanford University Medical Center where he is currently Professor of Radiology and Chief of Abdominal Imaging. In addition, he has served as Associate Dean for Academic Affairs, and is currently Associate Chair of Academic Affairs and Vice Chair for the Department. Dr. Jeffrey's main academic and research interests are in cross-sectional imaging of the abdomen, specifically focusing on CT and sonography, as well as thyroid imaging and biopsy. He is past president of the Society for Computed Body Tomography and Magnetic Resonance. He has authored over 300 peer-reviewed journal articles, 90 book chapters, and 10 textbooks dealing with abdominal imaging, the latest being the highly successful *DI Abdomen* and *DI Emergency*, both of which feature an imaging-focused design that has become the cutting-edge in radiology textbooks. Dr. Jeffrey was a co-recipient of the Magna Cum Laude Award for Scientific Exhibit at the RSNA in 1992 dealing with CT angiography. He was a member of the editorial board of *Radiology* from 1992 to 1997 and is currently a consultant to the editor of *Radiology*, and on the editorial board of *Ultrasound International* and *Journal of Clinical Ultrasound*. From 1999 to 2000, Dr. Jeffrey was a principal investigator for a $1.4 million, 4-year NIH Grant dealing with virtual colonoscopy. His current areas of research include advanced computer applications of CT, including 3-D imaging and virtual reality applications of spiral CT, as well as new ultrasound imaging applications for the liver, pancreas, and thyroid.

Butrus (Pierre) T. Khuri-Yakub is a Professor of Electrical Engineering at Stanford University, Stanford, CA. He received the B.S. degree in 1970 from the American University of Beirut, the M.S. degree in 1972 from Dartmouth College, Hanover, NH, and the Ph.D. degree in 1975 from Stanford University, all in electrical engineering. He was a Research Associate (1975–1978) then Senior Research Associate (1978–1982) at the E. L. Ginzton Laboratory of Stanford University and was promoted to the rank of Professor of Electrical Engineering in 1982. His current research interests include medical ultrasound imaging and therapy, micromachined ultrasonic transducers, smart bio-fluidic channels, microphones, ultrasonic fluid ejectors, and ultrasonic nondestructive evaluation, imaging, and microscopy. He has authored over 400 publications and has been principal inventor or co-inventor of 76 U.S. and internationally issued patents. He was awarded the Medal of the City of Bordeaux in 1983 for his contributions to nondestructive evaluation, the Distinguished Advisor Award of the School of Engineering at Stanford University in 1987, the Distinguished Lecturer Award of the IEEE UFFC society in 1999, a Stanford University Outstanding Inventor Award in 2004, and a Distinguished Alumnus Award of the School of Engineering of the American University of Beirut in 2005.